ISSN 1674-1056
http://cpb.iphy.ac.cn
http://iopscience.iop.org/cpb
中国物理 B
Chinese Physics
中国物理 Chinese Physics B

Epitaxial growth and transport properties of compressively-strained Ba_2IrO_4 films

Yun-Qi Zhao(赵蕴琦), Heng Zhang(张衡), Xiang-Bin Cai(蔡祥滨), Wei Guo(郭维), Dian-Xiang Ji(季殿祥), Ting-Ting Zhang(张婷婷), Zheng-Bin Gu(顾正彬), Jian Zhou(周健), Ye Zhu(朱叶), and Yue-Feng Nie(聂越峰)

Citation: Chin. Phys. B, 2021, 30 (**8**): 087401. DOI: 10.1088/1674-1056/abea97
Journal homepage: http://cpb.iphy.ac.cn; http://iopscience.iop.org/cpb

What follows is a list of articles you may be interested in

Two-dimensional square-Au_2S monolayer: A promising thermoelectric material with ultralow lattice thermal conductivity and high power factor

Wei Zhang(张伟), Xiao-Qiang Zhang(张晓强), Lei Liu(刘蕾), Zhao-Qi Wang(王朝棋), and Zhi-Guo Li(李治国)
Chin. Phys. B, 2021, 30 (**7**): 077405. DOI: 10.1088/1674-1056/abe115

Anomalous magnetoresistance in detwinned $EuFe_2As_2$

Zhuang Xu(徐状), Junxiang Pan(潘俊香), Zhen Tao(陶镇), Ruixian Liu(刘瑞鲜), Guotai Tan(谈国太)
Chin. Phys. B, 2020, 29 (**7**): 077402. DOI: 10.1088/1674-1056/ab90e4

Topological superconductivity in a $Bi_2Te_3/NbSe_2$ heterostructure: A review

Hao Zheng(郑浩), Jin-Feng Jia(贾金锋)
Chin. Phys. B, 2019, 28 (**6**): 067403. DOI: 10.1088/1674-1056/28/6/067403

Superconductivity of bilayer titanium/indium thin film grown on SiO_2/Si (001)

Zhao-Hong Mo(莫钊洪), Chao Lu(路超), Yi Liu(刘毅), Wei Feng(冯卫), Yun Zhang(张云), Wen Zhang(张文), Shi-Yong Tan(谭世勇), Hong-Jun Zhang(张宏俊), Chun-Yu Guo(郭春煜), Xiao-Dong Wang(汪小冬), Liang Wang(王亮), Rui-Zhu Yang(杨蕊竹), Zhong-Guo Ren(任忠国), Xie-Gang Zhu(朱燮刚), Zhong-Hua Xiong(熊忠华), Qi An(安琪), Xin-Chun Lai(赖新春)
Chin. Phys. B, 2018, 27 (**6**): 067403. DOI: 10.1088/1674-1056/27/6/067403

Electronic structure and nematic phase transition in superconducting multiple-layer FeSe films grown by pulsed laser deposition method

Bing Shen(沈兵), Zhong-Pei Feng(冯中沛), Jian-Wei Huang(黄建伟), Yong Hu(胡勇), Qiang Gao(高强), Cong Li(李聪), Yu Xu(徐煜), Guo-Dong Liu(刘国东), Li Yu(俞理), Lin Zhao(赵林), Kui Jin(金魁), X J Zhou(周兴江)
Chin. Phys. B, 2017, 26 (**7**): 077402. DOI: 10.1088/1674-1056/26/7/077402

Epitaxial growth and transport properties of compressively-strained Ba_2IrO_4 films*

Yun-Qi Zhao(赵蕴琦)[1,†], Heng Zhang(张衡)[1,†], Xiang-Bin Cai(蔡祥滨)[2], Wei Guo(郭维)[1], Dian-Xiang Ji(季殿祥)[1], Ting-Ting Zhang(张婷婷)[1], Zheng-Bin Gu(顾正彬)[1], Jian Zhou(周健)[1,‡], Ye Zhu(朱叶)[3,§], and Yue-Feng Nie(聂越峰)[1,¶]

[1] *National Laboratory of Solid State Microstructures, College of Engineering and Applied Sciences, and Collaborative Innovation Center of Advanced Microstructures, Nanjing University, Nanjing* 210093, *China*

[2] *Department of Physics, The Hong Kong University of Science and Technology, Clear Water Bay, Kowloon, Hong Kong, China*

[3] *Department of Applied Physics, Research Institute for Smart Energy, The Hong Kong Polytechnic University, Hung Hom, Kowloon, Hong Kong, China*

(Received 8 January 2021; revised manuscript received 7 February 2021; accepted manuscript online 1 March 2021)

Ba_2IrO_4 is a sister compound of the widely investigated Sr_2IrO_4 and has no IrO_6 octahedral rotation nor net canted antiferromagnetic moment, thus it acts as a system more similar to the high-T_c cuprate. In this work, we synthesize the Ba_2IrO_4 epitaxial films by reactive molecular beam epitaxy and study their crystalline structure and transport properties under biaxial compressive strain. High resolution scanning transmission electron microscopy and x-ray diffraction confirm the high quality of films with partial strain relaxation. Under compressive epitaxial strain, the Ba_2IrO_4 exhibits the strain-driven enhancement of the conductivity, consistent with the band gap narrowing and the stronger hybridization of Ir-t_{2g} and O-2p orbitals predicted in the first-principles calculations.

Keywords: molecular beam epitaxy, iridate oxides, epitaxial strain, transport properties

PACS: 74.70.–b, 74.78.–w **DOI:** 10.1088/1674-1056/abea97

1. Introduction

The strong spin–orbit coupling and its interplay with electron correlations in 5d transition metal oxides (TMOs) give rise to the intriguing $J_{\rm eff} = 1/2$ antiferromagnetic Mott insulator state in layered perovskite iridate Sr_2IrO_4.[1–3] The Sr_2IrO_4 possesses many common key signatures of superconductivity with the high T_c cuprates, such as Fermi arcs,[4,5] antiferromagnetic Mott ground state,[6] d-wave band gap, *etc*.[7–10] As such, Sr_2IrO_4 is predicted to be a new type of high-temperature superconductor upon electron-doping.[11,12] However, it is difficult to effectively dope enough charge carriers into Sr_2IrO_4 and drive them into the potential superconducting state.[13–17] In contrast to Sr_2IrO_4, the Ba_2IrO_4 (BIO) exhibits no IrO_6 octahedral rotations nor net canted ferromagnetic moments in the IrO_2 planes, thus it is more similar to the parent compound of high T_c cuprates.[18] However, the synthesis of large single crystal BIO is challenging as it is metastable in bulk and requires a high-pressure technique.[18] The syntheses of BIO thin films by pulsed laser deposition (PLD)[19] and molecular beam epitaxy (MBE)[20] were previously reported. The metal–insulator (M–I) transition has been observed in BIO under high pressure.[21] Experimental researches have demonstrated that epitaxial strains can tune the electronic structure of Sr_2IrO_4,[22] but the strain effects on Ba_2IrO_4 films remain unclear.

In this work, we synthesize Ba_2IrO_4 epitaxial films by reactive MBE and investigate their crystalline structures, transports, and electronic properties by x-ray diffraction (XRD), scanning transmission electron microscopy (STEM), and first-principles calculations.

2. Experiment

The BIO films were epitaxially grown on various single-crystal substrates by reactive MBE (DCA R450) with an oxidant (distilled O_3) background pressure of 5×10^{-6} Torr (1 Torr = 1.33322×10^2 Pa) and at a substrate temperature of 800 °C.[20] Barium flux wase generated by using a Knut effusion cell and iridium flux was produced by using an electron-beam evaporator due to its high evaporation temperature. Owning to the volatility of IrO_x, the BIO films were grown in the adsorption-controlled mode.[23] Since the BIO films were found to degrade quickly in humid air, we capped the BIO

*Project supported by the National Natural Science Foundation of China (Grant Nos. 11774153, 11861161004, 51772143, 11974163, and 51672125), the National Key Research and Development Program of China (Grant No. 2016YFA0201104), the Fundamental Research Funds for the Central Universities, China (Grant Nos. 0213-14380167 and 0213-14380198), and the Hong Kong Research Grants Council (RGC) through the NSFC–RGC Joint Research Scheme, China (Grant No. N_PolyU531/18).

†These authors contributed equally to this work.

‡Corresponding author. E-mail: zhoujian@nju.edu.cn

§Corresponding author. E-mail: yezhu@polyu.edu.hk

¶Corresponding author. E-mail: ynie@nju.edu.cn

© 2021 Chinese Physical Society and IOP Publishing Ltd

films with 10 unit cell (u.c.) $SrTiO_3$, which could protect the BIO films from being moisturized in ambient conditions.

To explore the strain effects, in the present study, three different single-crystal substrates were used, namely (001) $(LaAlO_3)_{0.3}(Sr_2AlTaO_6)_{0.7}$ (LSAT), (001) $SrTiO_3$ (STO), and (110) $GdScO_3$ (GSO). Bulk BIO is in a tetragonal phase with $a = 4.030$ Å and $c = 13.333$ Å.[18] The pseudo-cubic lattice parameters of the substrates and their nominal lattices mismatched with those of BIO are listed in Table 1. The optimal growth condition of BIO films strongly depends on the substrate. We obtained high quality BIO films on STO and GSO substrates but only poor-quality BIO films with impurity phases on the LSAT substrates. By growing a buffer layer of 5 u.c. of STO high quality BIO films are obtained on LSAT substrates. We also found that first deposition of a BaO layer on the substrate before co-depositing Ba and Ir species could greatly improve the film quality and this method is used for all BIO films studied in this work. This can be related to the volatility of IrO_x and an *A*-site terminated surface will be favorable for the absorption of IrO_x, but the exact underlying mechanism is more complicated. The BIO films in this work were all about 15-nm thick.

Table 1. Lattice parameters, lattice mismatches, and epitaxial strains of BIO films grown on various substrates. In the table, a_{sub} of GSO is a pseudo-cubic lattice constant, lattice mismatch $(\%) = (a_{sub} - a_{bulk})/a_{sub} \times 100\%$, $\varepsilon_{xx} = (a_{film} - a_{bulk})/a_{bulk} \times 100\%$.

Substrate	In-plane a_{sub} (Å)	Lattice mismatch (%)	a_{BIO} (Å)	c_{BIO} (Å)	ε_{xx} (%)
GSO (110)	3.96	–1.77	4.00	13.30	–0.74
STO (100)	3.90	–3.33	3.98	13.40	–1.24
LSAT (100)	3.87	–4.13	3.99	13.34	–0.99

The crystal structure of BIO films was characterized by high-resolution four-circle XRD using Bruker D8 Discover with Cu-K_α radiation. The STEM measurements were performed by JEOL ARM 200CF with the ASCOR probe corrector to investigate the microstructures of cross-sectional BIO films. High-angle annular dark field (HAADF) images are conducted with a 26-mrad convergence semi-angle and a 110-mrad inner collection semi-angle. Temperature-dependent electronic transport properties were measured by a conventional four-probe approach using the Van der Pauw method. The density functional theory (DFT) calculations were also performed to investigate the stain-driven electronic structure evolution.

3. Results and discussion

Figure 1(a) shows the crystal structure of BIO. The films are grown on three different substrates and undergo compressive strain imposed by substrates. The XRD 2θ–ω scans of the BIO films exhibit sharp (00l) peaks as shown in Fig. 1(b), indicating the high crystalline quality of the single crystal BIO films. To obtain the in-plane lattice constants and strain states of the films, we perform reciprocal space mapping (RSM). As shown in Fig. 2, the RSMs for all BIO films around the $(103)_p$ plane of substrates indicate that the H values of all the BIO films deviate from the H value of the substrates indicating the partial relaxation of the in-plane strain due to the large lattice mismatches. The detailed lattice mismatch, in-plane (a) and out-of-plane (c) lattice parameters determined from RSM are listed in Table 1. The residual strain state results from the combination of lattice mismatch and strain relaxation. The estimated residual in-plane compressive strains ε_{xx} is calculated from $\varepsilon_{xx} = [a_{film} - a_{bulk})/a_{bulk}] \times 100\%$. For the BIO films grown on GSO and STO substrates, the effective compressive strain increases with larger lattice mismatch increasing. However, for the BIO films grown on the LSAT, the strain is almost fully relaxed since the lattice mismatch (-4.13%) is too large. Note that a 10-u.c.-thick capping layer STO is deposited on all films in order to protect the BIO layer, which may contribute to the final strain states in the BIO films. Also, like the rocking curves, the width of the diffraction peaks along the H axis in the HL reciprocal space mapping also reflects the distribution of the crystal orientations. As shown in Fig. 2, the widths of the BIO peaks along H axis are similar to those of the substrates, indicating the high crystalline quality of the films.

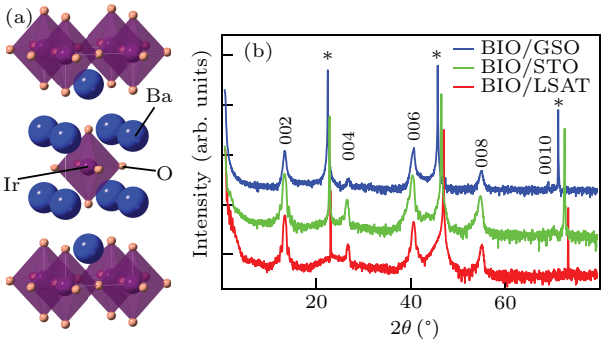


Fig. 1. (a) Schematic structure of bulk Ba_2IrO_4. (b) XRD 2θ–ω scans of BIO films grown on various substrates, with asterisks (*) corresponding to diffraction peaks of substrates. Note that BIO/LSAT film has a 5-u.c. STO as the buffer layer in order to grow high-quality BIO film on LSAT substrate.

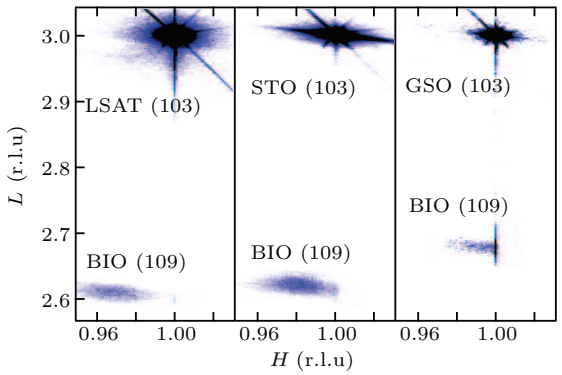


Fig. 2. Reciprocal space mapping (RSM) of BIO (109) diffractions near pseudo-cubic (103) diffractions of LSAT, STO, and GSO substrates. Note that BIO/LSAT film has a 5-u.c. STO as a buffer layer in order to grow high-quality BIO film on LSAT substrate.

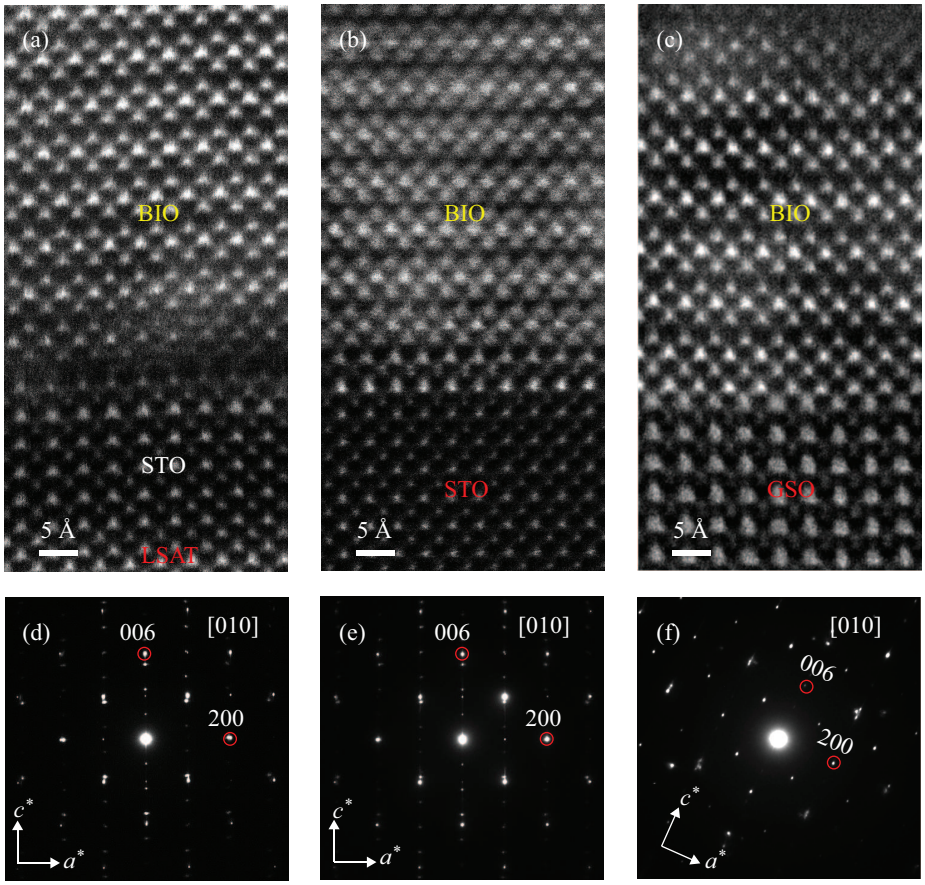


Fig. 3. (a)–(c) Cross-sectional STEM-ADF images projected along [010] direction near BIO/substrate interfaces, (d)–(f) selected-area electron diffraction patterns of the observed areas. Note that BIO/LSAT film has a 5-u.c. STO as buffer layer in order to grow high-quality BIO film on LSAT substrate.

High-resolution STEM annular dark field (ADF) images on the cross-section samples of BIO/substrate interfaces along the [010] zone axis are shown in Figs. 3(a)–3(c). The STEM-ADF images show the high-quality stacking of BaO and IrO_2 layers, which is consistent with the atomic crystal structure depicted in Fig. 1(a). The selected-area electron diffraction patterns (Figs. 3(d)–3(f)) also show sharp and bright diffractions of the BIO structure.

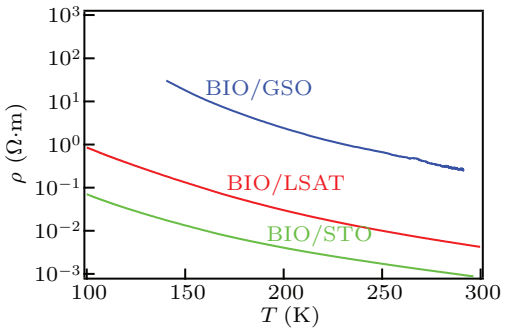


Fig. 4. Measured resistivity *versus* temperature of BIO films. Note that BIO/LSAT film has a 5-u.c. STO as buffer layer in order to grow high-quality BIO film on LSAT substrate.

Figure 4 shows the resistivities as a function of temperature of BIO films grown on three different substrates. All samples show a typical insulating behavior with negative $\mathrm{d}\rho/\mathrm{d}T$. The values of effective compressive strains are indicated in the inset. The resistivities of BIO films show clearly their dependence on the effective strain, namely the higher the compressive strain, the lower the resistivity will be.

To understand the strain effects on the transport behaviors in BIO films, we perform the calculations by using the first-principles density functional theory (DFT) with a generalized gradient approximation implemented in the Vienna *ab initio* simulation package (VASP) code,[24,25] in which the projected augmented wave method[26,27] and the Perdew–Burke–Ernzerhof revised for solids exchange-correlation functional[28] are used. The plane-wave cutoff energy is 520 eV throughout the calculations. The smallest spacing between the k-points is 0.2 Å^{-1} (KSPACING = 0.2). A $\sqrt{2}\times\sqrt{2}\times 1$ supercell is used to accommodate the antiferromagnetic structure in BIO. The electron correlation of the Ir ions is considered by the DFT+U scheme with the effective Hubbard $U = 2.0$ eV. Owing to the heavy Ir ions, the spin–orbital coupling (SOC) effect is also added into our calculations. The lattice constants and atomic positions are both relaxed to simulate the unstrained bulk BIO and the final optimized lattice constants are $a = 4.001$ Å and $c = 13.283$ Å, which are well consistent with the experimental results. Then the in-plane compressing effect is simulated by reducing the lattice constant (a) with a fixed ratio of 1%, and 2% while the out-of-plane lattice constant (c) and atomic positions are free to be relaxed.

As shown in Fig. 5, the total density of states (DOS) of BIO indicates a clear energy gap near the Fermi energy (red dash line) for the unstrained condition. The band gap gradually shrinks and disappears at an in-plane strain of −2%. This tendency is in accordance with transport experimental results that the conductivity of BIO film increases with in-plane compressive strain increasing. Projected-DOS on O-2p orbital, iridating t_{2g} and e_g orbitals are also shown in Fig. 5. The orbital characteristics of the electronic states near the Fermi level are dominated by Ir-t_{2g} and O-2p, exhibiting clearly that the stronger hybridization of these orbitals is enhanced with compressive strains applied. As a consequence, this narrows the band gap and increases the conductivity of BIO film under compressive strain as observed in our transport measurements.

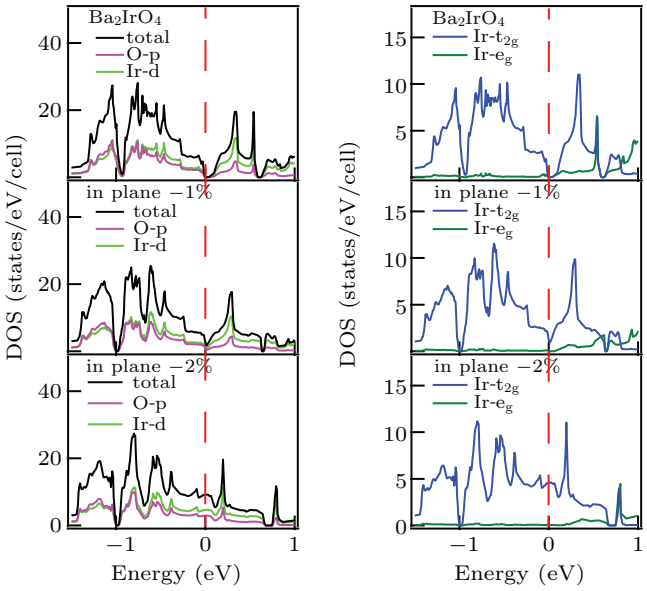


Fig. 5. Total and projected densities of states (DOSs) of BIO, showing a gap closing and increase of DOS under in-plane compressive strain. The dash line refers to Fermi energy.

4. Conclusions

In this work, we grow epitaxial Ba_2IrO_4 films on LSAT, STO, and GSO substrates by reactive MBE, and through the XRD and STEM structure characterizations confirm that all films have high crystalline quality. Three different strain states are achieved on these substrates with partial strain relaxation due to the relatively large lattice mismatch. The transport measurements show an enhancement of the conductivity by increasing in-plane compressive strains. The DFT calculations are consistent with our experimental results, and show that a band gap narrows and the hybridization between Ir-t_{2g} and O-2p orbitals increases under stronger compressive strain.

Acknowledgement

The numerical calculations in this paper were carried out on the computing facilities in the High-Performance Computing Center (HPCC) of Nanjing University.

References

[1] Kim B J, Jin H, Moon S J, Kim J Y, Park B G, Leem C S, Yu J, Noh T W, Kim C, Oh S J, Park J H, Durairaj V, Cao G and Rotenberg E 2008 *Phys. Rev. Lett.* **101** 076402
[2] Kim B J, Ohsumi H, Komesu T, Sakai S, Morita T, Takagi H and Arima T 2009 *Science* **323** 1329
[3] Xu H, Cui Z Z, Zhai X F and Lu Y L 2019 *Chin. Phys. B* **28** 078102
[4] Kim Y K, Krupin O, Denlinger J D, Bostwick A, Rotenberg E, Zhao Q, Mitchell J F, Allen J W and Kim B J 2014 *Science* **345** 187
[5] De la Torre A, McKeown Walker S, Bruno F Y, Riccó S, Wang Z, Gutierrez Lezama I, Scheerer G, Giriat G, Jaccard D, Berthod C, Kim T K, Hoesch M, Hunter E C, Perry R S, Tamai A and Baumberger F 2015 *Phys. Rev. Lett.* **115** 176402
[6] Kim J, Casa D, Upton M H, Gog T, Kim Y-J, Mitchell J F, van Veenendaal M, Daghofer M, van den Brink J, Khaliullin G and Kim B J 2012 *Phys. Rev. Lett.* **108** 177003
[7] Kim Y K, Sung N H, Denlinger J D and Kim B J 2016 *Nat. Phys.* **12** 37
[8] Yan Y J, Ren M Q, Xu H C, Xie B P, Tao R, Choi H Y, Lee N, Choi Y J, Zhang T and Feng D L 2015 *Phys. Rev. X* **5** 041018
[9] Zhao L, Torchinsky D H, Chu H, Ivanov V, Lifshitz R, Flint R, Qi T, Cao G and Hsieh D 2016 *Nat. Phys.* **12** 32
[10] Battisti I, Bastiaans K M, Fedoseev V, De la Torre A, Iliopoulos N, Tamai A, Hunter E C, Perry R S, Zaanen J, Baumberger F and Allan M P 2017 *Nat. Phys.* **13** 21
[11] Wang F and Senthil T 2011 *Phys. Rev. Lett.* **106** 136402
[12] Watanabe H, Shirakawa T and Yunoki S 2013 *Phys. Rev. Lett.* **110** 027002
[13] Cosio-Castaneda C, Tavizon G, Baeza A, De la Mora P and Escudero R 2007 *J. Phys.: Condens. Matter* **19** 446210
[14] Korneta O B, Qi T, Chikara S, Parkin S, De Long L E, Schlottmann P and Cao G 2010 *Phys. Rev. B* **82** 115117
[15] Haskel D, Fabbris G, Zhernenkov M, Kong P P, Jin C Q, Cao G and van Veenendaal M 2012 *Phys. Rev. Lett.* **109** 027204
[16] Souri M, Connell J G, Nichols J, Terzic J, Cao G and Seo A 2019 *J. Appl. Phys.* **126** 185101
[17] Guo W, Ji D X, Gu Z B, Zhou J, Nie Y F and Pan X Q 2020 *Phys. Rev. B* **101** 085101
[18] Okabe H, Isobe M, Takayama-Muromachi E, Koda A, Takeshita S, Hiraishi M, Miyazaki M, Kadono R, Miyake Y and Akimitsu J 2011 *Phys. Rev. B* **83** 155118
[19] Nichols J, Korneta O B, Terzic J, Cao G, Brill J W and Seo S S A 2014 *Appl. Phys. Lett.* **104** 121913
[20] Uchida M, Nie Y F, King P D C, Kim C H, Fennie C J, Schlom D G and Shen K M 2014 *Phys. Rev. B* **90** 075142
[21] Okabe H, Takeshita N, Isobe M, Takayama-Muromachi E, Muranaka T and Akimitsu J 2011 *Phys. Rev. B* **84** 115127
[22] Nichols J, Terzic J, Bittle E G, Korneta O B, De Long L E, Brill J W, Cao G and Seo S S A 2013 *Appl. Phys. Lett.* **102** 141908
[23] Cordfunke E H P and Meyer G 1962 *Recl. Trav. Chim. Pays-Bas* **81** 495
[24] Kresse G and Furthmüller J 1996 *Comput. Mater. Sci.* **6** 15
[25] Kresse G and Furthmüller J 1996 *Phys. Rev. B* **54** 11169
[26] Blöchl P E 1994 *Phys. Rev. B* **50** 17953
[27] Kresse G and Joubert D 1999 *Phys. Rev. B* **59** 1758
[28] Perdew J P, Ruzsinszky A, Csonka G I, Vydrov O A, Scuseria G E, Constantin L A, Zhou X and Burke K 2008 *Phys. Rev. Lett.* **100** 136406